Title

Diagnosis of spinal lesions using perfusion parameters measured by DCE-MRI and metabolism parameters measured by PET/CT

Journal

European Spine Journal, 29(5)

ISSN

0940-6719

Authors

Zhang, Jiahui
Chen, Yongye
Zhang, Yanyan
et al.

Publication Date

2020-05-01

DOI

10.1007/s00586-019-06213-9

Peer reviewed

HHS Public Access

Author manuscript

Eur Spine J. Author manuscript; available in PMC 2020 December 02.

Published in final edited form as:

Eur Spine J. 2020 May ; 29(5): 1061–1070. doi:10.1007/s00586-019-06213-9.

Diagnosis of Spinal Lesions Using Perfusion Parameters Measured by DCE-MRI and Metabolism Parameters Measured by PET/CT

Jiahui Zhang[1], **Yongye Chen**[1], **Yanyan Zhang**[2], **Enlong Zhang**[1], **Hon J. Yu**[3], **Huishu Yuan**[1], **Yang Zhang**[3], **Min-Ying Su**[3,*], **Ning Lang**[1,**]

[1]Department of Radiology, Peking University Third Hospital, Beijing, China

[2]Department of Nuclear Medicine, Peking University Third Hospital, Beijing, China

[3]Department of Radiological Sciences, University of California, Irvine, CA, USA

Abstract

Objective: To investigate the correlation of parameters measured by dynamic-contrast-enhanced MRI (DCE-MRI) and ^{18}F-FDG PET/CT in spinal tumors, and their role in differential diagnosis.

Methods: A total of 49 patients with pathologically confirmed spinal tumors, including 38 malignant, 6 benign, and 5 borderline tumors, were analyzed. The MRI and PET/CT were done within 3 days, before biopsy. On MRI, the ROI was manually placed on area showing the strongest enhancement to measure pharmacokinetic parameters K^{trans} and k_{ep}. On PET, the maximum standardized uptake value SUV_{max} was measured. The parameters in different histological groups were compared. ROC was performed to differentiate between the two largest subtypes, metastases and plasmacytomas. Spearman rank correlation was performed to compare DCE-MRI and PET/CT parameters.

Results: The K^{trans}, k_{ep} and SUV_{max} were not statistically different among malignant, benign and borderline groups (P= 0.95, 0.50, 0.11). There was no significant correlation between K^{trans} and SUV_{max} (r= −0.20, P=0.18), or between k_{ep} and SUV_{max} (r= −0.16, P=0.28). The k_{ep} was significantly higher in plasmacytoma than in metastasis (0.78±0.17 vs. 0.61±0.18, P=0.02); and in contrast, the SUV_{max} was significantly lower in plasmacytoma than in metastasis (5.58±2.16 vs. 9.37±4.26, P=0.03). In differential diagnosis, the AUC of k_{ep} and SUV_{max} were 0.79 and 0.78, respectively.

Conclusions: The vascular parameters measured by DCE-MRI and glucose metabolism measured by PET/CT from the most aggressive tumor area did not show a significant correlation. The results suggest they provide complementary information reflecting different aspects of the tumor, which may aid in diagnosis of spinal lesions.

[*]**Corresponding Author: Min-Ying Su, PhD (in United States)**, 164 Irvine Hall, Center for Functional Onco-Imaging, University of California, Irvine, CA 92697-5020. Tel: +1 (949) 824-4925, Fax: +1 (949) 824-3481, msu@uci.edu. [**]**Corresponding Author: Ning Lang, MD (in China)**, Department of Radiology, Peking University Third Hospital, 49 North Garden Road, Haidian District, Beijing, 100191, PR China. Tel: +86 10 82264292; Fax: +86 10 62017700, langning800129@126.com.

Keywords

Magnetic Resonance Imaging; Positron Emission Tomography Computed Tomography; Spinal Neoplasms

Introduction

Magnetic resonance imaging (MRI) is often recommended for patients presenting with pain in the spine, who are suspected to have lesions compressing the spinal cord. The most likely malignancy is metastatic cancer and primary bone tumor. Borderline tumors (locally aggressive and rarely metastasizing) and benign lesions are also found in the spine, and each lesion needs to be correctly diagnosed to decide the most appropriate treatment plan. Although MRI can provide detailed morphological information about the deformation of bone and the presence of soft tissue lesion, there are no specific imaging features that can be used to diagnose different types of lesions. Several studies have shown that the vascular parameters measured by dynamic-contrast-enhanced MRI (DCE-MRI) can provide additional information to help differentiation of lesions in the spine, e.g. primary bone cancers such as myeloma, lymphoma, chordoma, giant cell tumor of the bone [1–4]; benign lesions such as tuberculosis [5]; and metastatic cancers of different primary [6–8].

For patients suspecting to have malignant lesions in the spine, the ^{18}F-fluorodeoxyglucose (FDG) positron emission tomography/ computed tomography (PET/CT) is another commonly used imaging modality. In addition to detecting malignancy, it is also used for staging to evaluate the extent of disease, monitoring treatment response, and predicting prognosis [9, 10]. FDG is transported by glucose transporters and metabolized by the enzyme hexokinase, so a high uptake is seen in malignant cancer cells but it may also occur in tissues with a high cellular proliferation, e.g. in aggressive benign tumors, inflammation and normal bone marrow.

Vascular properties measured by DCE-MRI and glucose metabolism measured by ^{18}F-FDG PET/CT may provide complementary information representing different aspects of the lesion. Their associations in lung cancer, head and neck cancer and atherosclerosis have been investigated before [11–16]. Their association in spinal lesions has not been reported yet, possibly due to lack of data because DCE-MRI is not included in the standard protocol for spinal MRI. A better understanding of the relationship between vascularity and glucose metabolism will help to explore their clinical implications in management of spinal diseases.

The purpose of this study was to investigate the imaging parameters measured by DCE-MRI and ^{18}F-FDG PET/CT in various spinal lesions, which were histologically confirmed as malignant, benign and borderline tumors. The association among the measured parameters, and their diagnostic role were analyzed.

Materials and Methods

Subjects

A total of 49 patients with spinal tumors who underwent DCE-MRI and PET/CT examinations from February 2014 to August 2017 were identified from a retrospective search of our imaging database. The mean age was 50.6 ± 15.5 years old, range 17 to 79 years old, 30 males and 19 females. These patients were referred to receive MRI and PET/CT for diagnosis, due to numbness of corresponding limb and pain caused by lesions compressing the spinal cord. Only cases with two imaging done within a few days, before biopsy, were included. The interval time between the two examinations was less than 3 days. The histological diagnosis of each lesion was confirmed by biopsy or surgical pathology, with a total of 38 malignant tumors (including 19 metastases and 8 primary plasmacytomas), 6 benign tumors, and 5 borderline tumors classified based on the WHO Classification of Tumors of Soft Tissue and Bone (Table 1). The borderline (or, intermediate) tumors are defined based on being locally aggressive or having rare chance of metastasis. The study was approved by the Ethics Committee of our hospital, and informed consent was waived.

MRI and PET/CT Imaging Protocol

The MRI was performed on a Siemens Trio 3.0T system (Siemens, Erlangen, Germany). The axial T2WI, coronal T2WI, sagittal T2WI, T1WI, and fat suppression T2WI images were acquired using the fast spin echo sequence. After the abnormal region was found, DCE-MRI was acquired using a FLASH 3D VIBE sequence, with TR=4.1ms, TE=1.5 ms, flip angle=10°, matrix=256×192, FOV (field of view) =250mm×250 mm, slice thickness=3mm. A total of 16 DCE time frames were taken covering the DCE time period of 120~168 s. The contrast agent, gadopentetate dimeglumine (Gd-DTPA), at a dose of 0.1 mmol/kg was injected after one pre-contrast frame was taken, with the speed of 2 ml/s.

PET/CT was performed using a Siemens Biograph 64 PET/CT system (Siemens, Erlangen, Germany) with 52-rings PET, and 64-row spiral CT. All patients were fasted before the examination, and blood glucose levels were in the range of 4.4–9.3 mmol/L. All patients underwent whole-body PET/CT conventional imaging 60 minutes after injection of 3.7–4.5 MBq/kg ^{18}F-FDG. A 64-row spiral CT scan was performed with voltage of 140 kV, current of 100 mA, and a slice thickness of 3 mm. PET imaging was done using the 3D mode acquisition with iterative construction. The scan time was 8 minutes for the head scan, and 3 minutes per bed for the body scan from calvaria to the upper part of the femur.

Image Analysis

For MRI analysis, the region of interest (ROI) of 0.5 to 1.2 cm^2 was manually placed on the area showing the strongest contrast enhancement, and avoiding cystic lesions, calcification, necrosis and hemorrhage. The signal intensity-time curve from this ROI was obtained using the Siemens Sygno Mean Curve software. Three heuristic parameters were calculated from each DCE time course: the steepest wash-in signal enhancement ratio [(S2-S1)/S0]; the maximum signal enhancement ratio [(Smax-S0)/S0]; and the wash-out slope [(Speak-Slast)/Speak] (or, if no peak [(S67s-Slast)/S67s]). The DCE time course was also analyzed with a 2-compartmental pharmacokinetic model to obtain K^{trans} (1/min) and k_{ep} (1/min), following

the previously reported method [3]. The correlation between heuristic parameters directly calculated from the DCE time course and the fitted pharmacokinetic parameters was evaluated. It was found that k_{ep} was highly correlated with wash-out slope (r=0.95), and K^{trans} was highly correlated with max SE ratio (r=0.99) and steepest wash-in SE ratio (r=0.92), as shown in the Figure included in the supplementary material. Therefore, only the pharmacokinetic parameters K^{trans} and k_{ep} were used in further analysis.

For PET analysis, the ROI was manually placed on the entire area showing high ^{18}F-FDG uptake, and the maximum standardized uptake value SUV_{max} within the ROI was measured. For patients who had abnormal findings in multiple spinal segments, only the lesion corresponding to that analyzed on MRI was considered.

Statistical analysis

The quantitative DCE-MRI parameters, K^{trans} and k_{ep}, and PET/CT parameter SUV_{max}, were analyzed using the SPSS 22.0 statistical software. Kruskal-Wallis H rank sum test were used to compare the statistical differences between the parameters in malignant, benign and borderline tumor groups. Mann-Whitney U rank sum test was used to compare between metastasis cancer and primary plasmacytoma groups, with P less than 0.05 as statistically significant. Spearman rank correlation analysis was used to compare the association of K^{trans} and k_{ep} with SUV_{max} in the entire group of 49 cases, and also in each subgroup. The diagnostic performance to differentiate between metastases and plasmacytomas was evaluated using receiver operating characteristic (ROC) curve. The area under the curve (AUC) was calculated, and then the optimal threshold of each parameter was determined according to the Youden index to obtain diagnostic sensitivity and specificity.

Results

Comparison in malignant, borderline and benign groups

The mean and standard deviation of each analyzed parameter in three groups, as well as in each histological subtype, are summarized in Table 1. The MRI and PET images of one renal metastasis and one plasmacytoma are shown in Figure 1 and Figure 2, respectively. The images from two benign lesions, Schwannoma and Hemangioma, are shown in Figure 3 and Figure 4, respectively. The values of K^{trans}, k_{ep} and SUV_{max} were not statistically different among the three subgroups of malignant, benign and borderline tumors, with P = 0.95, 0.50, and 0.11, respectively.

Association between DCE-MRI and PET/CT parameters

The scattered plot of K^{trans} vs. SUV_{max} and k_{ep} vs. SUV_{max} are shown in Figure 5, and cases in malignant, borderline and benign groups are separately marked. In the entire group of 49 cases, there was no significant association between K^{trans} and SUV_{max} (r = −0.20, P = 0.18) or between k_{ep} and SUV_{max} (r = −0.16, P = 0.28). Also, there was no significant association between K^{trans} and k_{ep} vs. SUV_{max} within each of three subgroups.

Differential diagnosis between metastasis and plasmacytoma

The parameters between the two largest pathological types: 19 metastatic tumors and 8 plasmacytomas, were compared, as also shown in Table 1. The mean k_{ep} was 0.78±0.17 in plasmacytoma, significantly higher than 0.61±0.18 in metastasis (P= 0.02). In contrast, SUV_{max} was 5.58±2.16 in plasmacytoma, significantly lower than 9.37±4.26 in metastasis (P =0.03). There was no significant difference between K^{trans} of these two histological subtypes (P =0.87). The ROC analysis results are shown in Table 2. The AUC was 0.79 for k_{ep} and 0.78 for SUV_{max}, respectively. The optimal threshold was decided based on the Youden Index, and the sensitivity and specificity to differentiate between them were 87.5% and 73.7% based on k_{ep}, and 78.9% and 62.5% based on SUV_{max}. The diagnostic performance between k_{ep} and SUV_{max} by Z test was not statistically significant (Z = 0.10, P = 0.92).

Discussion

The blood supply and glucose utilization is needed for all tumors to grow. Contrast-enhanced MRI can detect tumors with rich blood supply, but it cannot reveal detailed vascular properties such as vascular perfusion and permeability. DCE-MRI, by measuring the enhancement at different time points, can evaluate the delivery and wash-out of contrast agents into and out of the tumor, thus reflect the microvascular distribution within the tissue. The quantitative analysis using the two-compartmental pharmacokinetic Tofts model can obtain the in-flux and out-flux transfer constant K^{trans} and k_{ep}, which are related to the blood perfusion and vascular permeability of the tumor [3, 17]. ^{18}F-FDG PET/CT measures the glycolysis in tissues, and it is commonly used for detection and staging of unknown tumors or metastases in the whole-body, as well as for evaluation of treatment response and prognosis [9, 10]. The maximum standardized uptake value (SUV_{max}) is the most commonly analyzed parameter as a semi-quantitative indicator of glucose metabolism. Therefore, vascular parameters measured by DCE-MRI and the glucose metabolism parameters measured by ^{18}F-FDG PET/CT may assess different aspects of lesions.

There are no report of relationships between K^{trans}, k_{ep} and SUV_{max} values of spinal tumors published in the literature yet. The patients included in the study were those who had compliant of limb numbness and back pain, and referred to our hospital for imaging diagnosis. In the search of clinical database with both DCE-MRI and PET/CT within a few days before biopsy, a total of 49 patients with histologically confirmed spinal tumors were identified, and their images were extracted to perform the analysis. The results showed that there was no significant correlation between K^{trans}, k_{ep} and SUV_{max} in the entire group of 49 cases or in each of the malignant, borderline and benign subgroups, indicating that blood perfusion was not directly associated with glucose metabolism.

Several studies have investigated the relationships of parameters measured by DCE-MRI and FDG PET. Han et al. [15] studied head and neck squamous cell carcinoma (HNSCC) using multi-parametric MRI, including DCE and diffusion-weighted imaging (DWI), and PET/CT. Significant correlations among various MRI parameters were found, but not between MRI and PET parameters, suggesting that each diagnostic technique may provide complementary information for HNSCC. In two more recent studies for HNSCC, it was further found that

the complex correlations might be related to the pathological grade of tumors [12,14]. Feng et al. [13] studied 17 benign and 32 malignant solitary pulmonary nodules, and found a positive correlation between K^{trans} and k_{ep} with SUV_{max}. In their study, the ROI was drawn manually to contour the border of each lesion, which included the entire lesion, and thus the extracted parameters were the averaged value over the heterogeneous tissues. The heterogeneity within a tumor can be studied with pixel-based analysis. A study by Lee et al. [11] in non-small cell lung cancer found that the intratumoral heterogeneity in wash-in contrast kinetics of DCE-MRI was associated with tumor metabolism measured by PET. Other than tumors, Calcagno et al. [16] applied DCE-MRI and FDG PET to study the role of inflammation and neovascularization in vulnerable atherosclerotic plaques in patients with coronary heart disease. It was reported that complex relationship between plaque inflammation and microvascularization may vary during the different stages of plaque development. The case numbers reported in these studies were relatively small, which could be due to the difficulty to perform corresponding DCE-MRI and FDG PET studies in the same patients within a short time period.

In addition to the correlation analysis, several studies applied the combined DWI, DCE-MRI and FDG PET imaging to predict treatment response and prognosis, based on the different information that can be provided by each imaging modality. Wong et al. [18] reported that the early intra-tumor changes are predictive of ultimate response to chemoradiation in HNSCC patients to differentiate 27 responders from 8 non-responders. Similar studies have been performed to predict response in breast cancer patients receiving neoadjuvant chemotherapy [19, 20], and cervical cancer patients receiving chemoradiation therapy [21, 22]. Combined DCE-MRI and FDG PET have also been applied to predict prognosis. Chen et al. [23] found that flow-metabolism mismatch reflected by the total lesion glycolysis (TLG)/peak ratio in pancreatic cancer patients may better predict survival than other imaging biomarkers from PET/MRI. The combined parameters may also improve the stratification of survival in patients with oropharyngeal or hypopharyngeal squamous cell carcinoma (OHSCC) treated with chemoradiation [24,25]. Lim et al. [26] also reported that the changes after one cycle of neoadjuvant chemotherapy in breast cancer patients measured by combined DCE-MRI and FDG PET can predict disease-free survival.

All these studies support that the parameters measured by DCE-MRI and PET/CT reflect different histopathological features of the tumor, which can be combined for diagnosis, staging, and prediction of treatment response and prognosis. In the present study we reported the results of K^{trans}, k_{ep} and SUV_{max} in various spinal lesions, separated into 38 malignant, 6 benign and 5 borderline tumors. We found a wide distribution, even within the benign and borderline groups, which could be attributed to their different histopathological types and different degree of cellular differentiation. For example, the benign hemangioma case shown in Figure 4 had a high vascular supply, but a low FDG uptake. The multiple plasmacytoma case shown in Figure 2 involved multiple segments, but the high FDG uptake on C2 was not corresponding to a high contrast enhancement on MRI; and in contrast, the lesion showing a stronger enhancement on C5 had a lower FDG uptake. One benign tumor, the giant cell tumor of tendon sheath, had a very high $SUV_{max}>15$; and 4 of the borderline tumors also had a high $SUV_{max}>10$. Although these tumors are not malignant, they need to be detected and correctly diagnosed for deciding an optimal treatment plan, and as shown in this study

both MRI and PET may provide valuable information. The high FDG uptake is also commonly seen in inflammatory tissues, also in normal bone marrow (as shown in Figures 1 and 4).

We further studied the differentiation between the spinal metastasis and plasmacytoma groups, the two highest number of histological subtypes. The results showed that the SUV_{max} was significantly higher in metastasis than in plasmacytoma, and the k_{ep} was higher in plasmacytoma than in metastasis. The AUC based on these two parameters were 0.79 and 0.78, respectively. The results are reasonable, as a high glucose metabolism in metastatic cancer is anticipated, and plasmacytoma is known to have a rich blood perfusion.

Since patients in this study already had severe symptoms in the spine, surgery was performed in most of them, followed by appropriate radiation and chemotherapy needed for treating different malignancies. Therefore, in addition to being used to guide diagnosis, the measured information was also used for surgical planning. The major limitation of this study was the retrospective design and the small case number. More cases are needed to understand the corresponding role of MRI and PET features in management of spinal lesions.

In conclusion, we evaluated the relationship between DCE-MRI pharmacokinetic parameters, K^{trans} and k_{ep}, and ^{18}F-FDG PET/CT parameter, SUV_{max}, in spinal tumors, to provide preliminary results about their complementary role for understanding the biological characteristics. Based on the hot-spot analysis approach by manually placing ROI on the most aggressive tissue region, there was no significant correlation between blood perfusion and glucose metabolism parameters. The results suggest that the two diagnostic techniques using DCE-MRI and PET/CT can provide complementary information. For diagnostic purposes, although it is difficult to predict the likelihood of malignancy, the lesions are clearly visible on MRI and PET, which can provide useful information for guiding the workup procedure or biopsy to target the most aggressive area. When more cases are available, their combined value in making differential diagnosis for spinal lesions can be further studied.

Supplementary Material

Refer to Web version on PubMed Central for supplementary material.

Acknowledgements

This study was supported by National Natural Science Foundation of China (81701648 and 81871326), NIH R01 CA127927 and Key Clinical Projects of the Peking University Third Hospital (BYSY2018007).

List of Abbreviations:

AUC	Area Under the Curve
CT	Computed Tomography
DCE-MRI	Dynamic-Contrast-Enhanced Magnetic Resonance Imaging

DWI	Diffusion Weighted Imaging
FDG	Fluorodeoxyglucose
PET	Positron Emission Tomography
ROC	Receiver Operating Characteristic
ROI	Region Of Interest
SE	Signal Enhancement
SUV	Standardized Uptake Value
TR	Repetition Time
TE	Echo Time

References

1. Lang P, Honda G, Roberts T, Vahlensieck M, Johnston JO, Rosenau W, et al. (1995) Musculoskeletal neoplasm: perineoplastic edema versus tumor on dynamic postcontrast MR imaging with spatial mapping of instantaneous enhancement rates. Radiology 197:831–839 [PubMed: 7480764]
2. Moulopoulos LA, Maris TG, Papanikolaou N, Panagi G, Vlahos L, Dimopoulos MA (2003) Detection of malignant bone marrow involvement with dynamic contrast-enhanced magnetic resonance imaging. Ann Oncol 14(1):152–158 [PubMed: 12488307]
3. Lang N, Yuan H, Yu HJ, Su MY (2017) Diagnosis of Spinal Lesions Using Heuristic and Pharmacokinetic Parameters Measured by Dynamic Contrast-Enhanced MRI. Acad Radiol 24(7):867–875 [PubMed: 28162875]
4. Lang N, Su MY, Xing X, Yu HJ, Yuan H (2017) Morphological and dynamic contrast enhanced MR imaging features for the differentiation of chordoma and giant cell tumors in the Axial Skeleton. J Magn Reson Imaging 45(4):1068–1075 [PubMed: 27490009]
5. Lang N, Su MY, Yu HJ, Yuan H (2015) Differentiation of tuberculosis and metastatic cancer in the spine using dynamic contrast-enhanced MRI. Eur Spine J 24:1729–1737 [PubMed: 25749725]
6. Saha A, Peck KK, Lis E, Holodny AI, Yamada Y, Karimi S (2014) Magnetic resonance perfusion characteristics of hypervascular renal and hypovascular prostate spinal metastases: clinical utilities and implications. Spine 39:E1433–E1440 [PubMed: 25188594]
7. Khadem NR, Karimi S, Peck KK, Yamada Y, Lis E, Lyo J, et al. (2012) Characterizing hypervascular and hypovascular metastases and normal bone marrow of the spine using dynamic contrastenhanced MR imaging. AJNR Am J Neuroradiol 33:2178–2185 [PubMed: 22555585]
8. Lang N, Su MY, Yu HJ, Lin M, Hamamura MJ, Yuan H (2013) Differentiation of myeloma and metastatic cancer in the spine using dynamic contrast-enhanced MRI. Magn Reson Imaging 31:1285–1291 [PubMed: 23290477]
9. Dammacco F, Rubini G, Ferrari C,Vacca A, Racanelli V (2015) ^{18}F-FDG PET/CT: a review of diagnostic and prognostic features in multiple myeloma and related disorders. Clin Exp Med 15(1):1–18 [PubMed: 25218739]
10. Al-Ibraheem A, Buck A, Krause BJ, Scheidhauer K, Schwaiger M (2009) Clinical applications of FDG PET and PET/CT in head and neck cancer. J Oncol 2009:208725 [PubMed: 19707528]
11. Lee SH, Rimner A, Gelb E, Deasy JO, Hunt MA, Humm JL, Tyagi N (2018) Correlation Between Tumor Metabolism and Semiquantitative Perfusion Magnetic Resonance Imaging Metrics in Non-Small Cell Lung Cancer. Int J Radiat Oncol Biol Phys 102(4):718–726 [PubMed: 29680254]
12. Surov A, Leifels L, Meyer HJ, Winter K, Sabri O, Purz S (2018) Associations Between Histogram Analysis DCE MRI Parameters and Complex 18F-FDG-PET Values in Head and Neck Squamous Cell Carcinoma. Anticancer Res 38(3):1637–1642 [PubMed: 29491096]

13. Feng F, Qiang F, Shen A, Shi D, Fu A, Li H (2018) Dynamic contrast-enhanced MRI versus 18F-FDG PET/CT: Which is better in differentiation between malignant and benign solitary pulmonary nodules? Chinese Journal of Cancer Research 30(1):21–30 [PubMed: 29545716]
14. Leifels L, Purz S, Stumpp P, Schob S, Meyer HJ, Kahn T (2017) Associations between 18F-FDG-PET, DWI, and DCE parameters in patients with head and neck squamous cell carcinoma depend on tumor grading. Contrast Media Mol Imaging 2017:5369625 [PubMed: 29114177]
15. Han M, Kim S, Lee S, Choi JW (2015) The Correlations Between MRI Perfusion, Diffusion Parameters, and 18F-FDG PET Metabolic Parameters in Primary Head-and-Neck Cancer: A Cross-Sectional Analysis in Single Institute. Medicine 94(47):e2141. [PubMed: 26632740]
16. Calcagno C, Ramachandran S, Izquierdo-Garcia D, et al. (2013) The complementary roles of dynamic contrast-enhanced MRI and 18F-fluorodeoxyglucose PET/CT for imaging of carotid atherosclerosis. Eur J Nucl Med Mol Imaging 40(12):1884–1893 [PubMed: 23942908]
17. Tofts PS (1997) Modeling tracer kinetics in dynamic Gd-DTPA MR imaging. J Magn Reson Imaging 7(1): 91–101 [PubMed: 9039598]
18. Wong KH, Panek R, Dunlop A, Mcquaid D, Riddell A, Welsh LC, et al. (2018) Changes in multimodality functional imaging parameters early during chemoradiation predict treatment response in patients with locally advanced head and neck cancer. Eur J Nucl Med Mol Imaging 45(5):759–767 [PubMed: 29164301]
19. An YY, Kim SH, Kang BJ, Lee AW (2015) Treatment Response Evaluation of Breast Cancer after Neoadjuvant Chemotherapy and Usefulness of the Imaging Parameters of MRI and PET/CT. J Korean Med Sci 30(6):808–815 [PubMed: 26028936]
20. Cho N, Im SA, Cheon GJ, Park IA, Lee KH, Kim TY, et al. (2018) Integrated 18F-FDG PET/MRI in breast cancer: early prediction of response to neoadjuvant chemotherapy. Eur J Nucl Med Mol Imaging 45(3):328–339 [PubMed: 29101445]
21. Sarabhai T, Tschischka A, Stebner V, Nensa F, Wetter A, Kimmig R, et al. (2018) Simultaneous multiparametric PET/MRI for the assessment of therapeutic response to chemotherapy or concurrent chemoradiotherapy of cervical cancer patients: Preliminary results. Clin Imaging 49:163–168 [PubMed: 29554613]
22. Bowen SR, Yuh WTC, Hippe DS, Wu W, Partridge SC, Elias S, et al. (2018) Tumor radiomic heterogeneity: Multiparametric functional imaging to characterize variability and predict response following cervical cancer radiation therapy. J Magn Reson Imaging 47(5):1388–1396 [PubMed: 29044908]
23. Chen BB, Tien YW, Chang MC, Cheng MF, Chang YT, Yang SH, et al. (2018) Multiparametric PET/MR imaging biomarkers are associated with overall survival in patients with pancreatic cancer. Eur J Nucl Med Mol Imaging 45(7):1205–1217 [PubMed: 29476229]
24. Ng SH, Liao CT, Lin CY, Chan SC, Lin YC, Yen TC, et al. (2016) Dynamic contrast-enhanced MRI, diffusion-weighted MRI and 18F-FDG PET/CT for the prediction of survival in oropharyngeal or hypopharyngeal squamous cell carcinoma treated with chemoradiation. Eur Radiol 26(11):4162–4172 [PubMed: 26911889]
25. Chan SC, Cheng NM, Hsieh CH, Ng SH, Lin CY, Yen TC, et al. (2017) Multiparametric imaging using 18F-FDG PET/CT heterogeneity parameters and functional MRI techniques: prognostic significance in patients with primary advanced oropharyngeal or hypopharyngeal squamous cell carcinoma treated with chemoradiotherapy. Oncotarget 8(37):62606–62621 [PubMed: 28977973]
26. Lim I, Noh WC, Park J, Park JA, Kim HA, Kim EK, et al. (2014) The combination of FDG PET and dynamic contrast-enhanced MRI improves the prediction of disease-free survival in patients with advanced breast cancer after the first cycle of neoadjuvant chemotherapy. Eur J Nucl Med Mol Imaging 41(10):1852–1860 [PubMed: 24927797]

KEY POINTS

1. The vascular parameters measured by DCE-MRI and glucose metabolism measured by FDG PET/CT were not significantly correlated, suggesting they provide complementary information.
2. Metastatic cancers have a significantly higher SUV_{max} and a lower k_{ep} compared to plasmacytomas in the spine, with AUC approaching 0.8 in differentiation between these two subtypes.
3. For diagnostic purposes, although it is difficult to predict the likelihood of malignancy, the lesions are clearly visible on MRI and PET, which can provide useful information for guiding the subsequent workup procedure or biopsy.

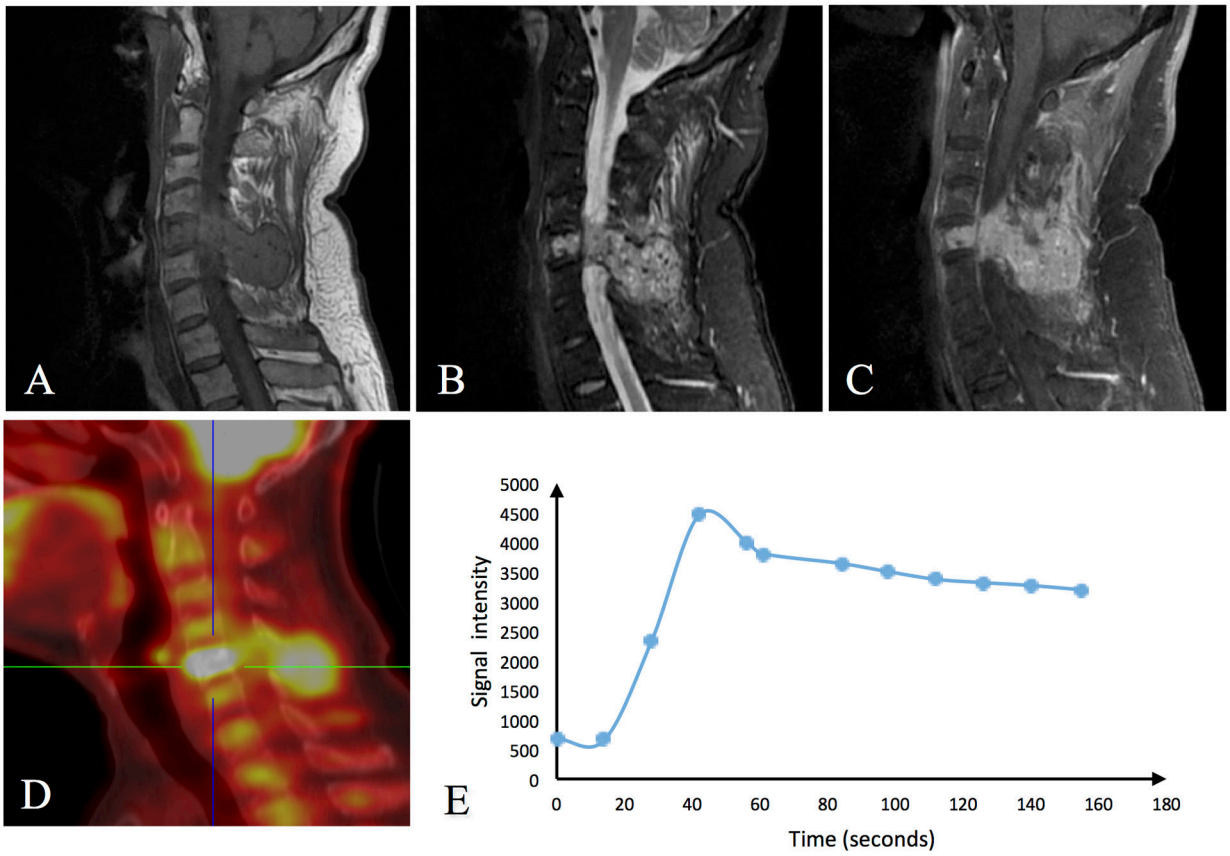

Figure 1.

A 52-year-old male patient with metastatic renal cancer on C5. (A) T1-weighted image; (B) T2-weighted fat-suppressed image; (C) T1-weighted contrast-enhanced image; (D) FDG uptake map; (E) DCE signal intensity time course. A strong FDG uptake is seen, with SUVmax=13.3, and the DCE kinetic shows the wash-out pattern with K^{trans}=0.55 (1/min) and k_{ep}=0.80 (1/min).

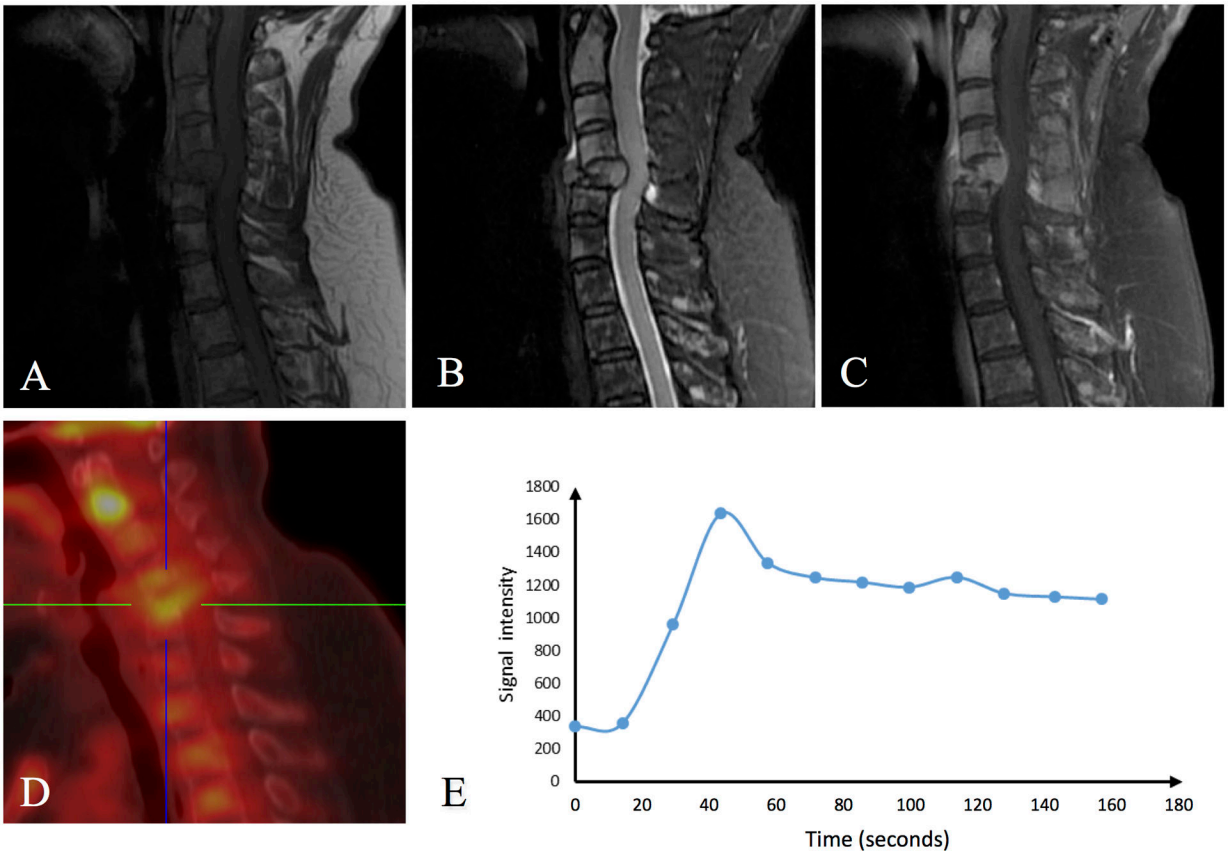

Figure 2.

A 64-year-old female patient with multiple plasmacytoma, showing obvious deformation on C5. (A) T1-weighted image; (B) T2-weighted fat-suppressed image; (C) T1-weighted contrast-enhanced image; (D) FDG uptake map; (E) DCE signal intensity time course. A high FDG uptake is seen on C2, but there is no clear abnormality shown on MRI. The lesion on C5 compresses the spinal cord, which is visible on both MRI and PET. The measured DCE time course from the enhanced lesion on C5 shows the wash-out pattern with K^{trans}=0.34 (1/min) and k_{ep}=0.82 (1/min), and the measured SUV_{max}=6.1.

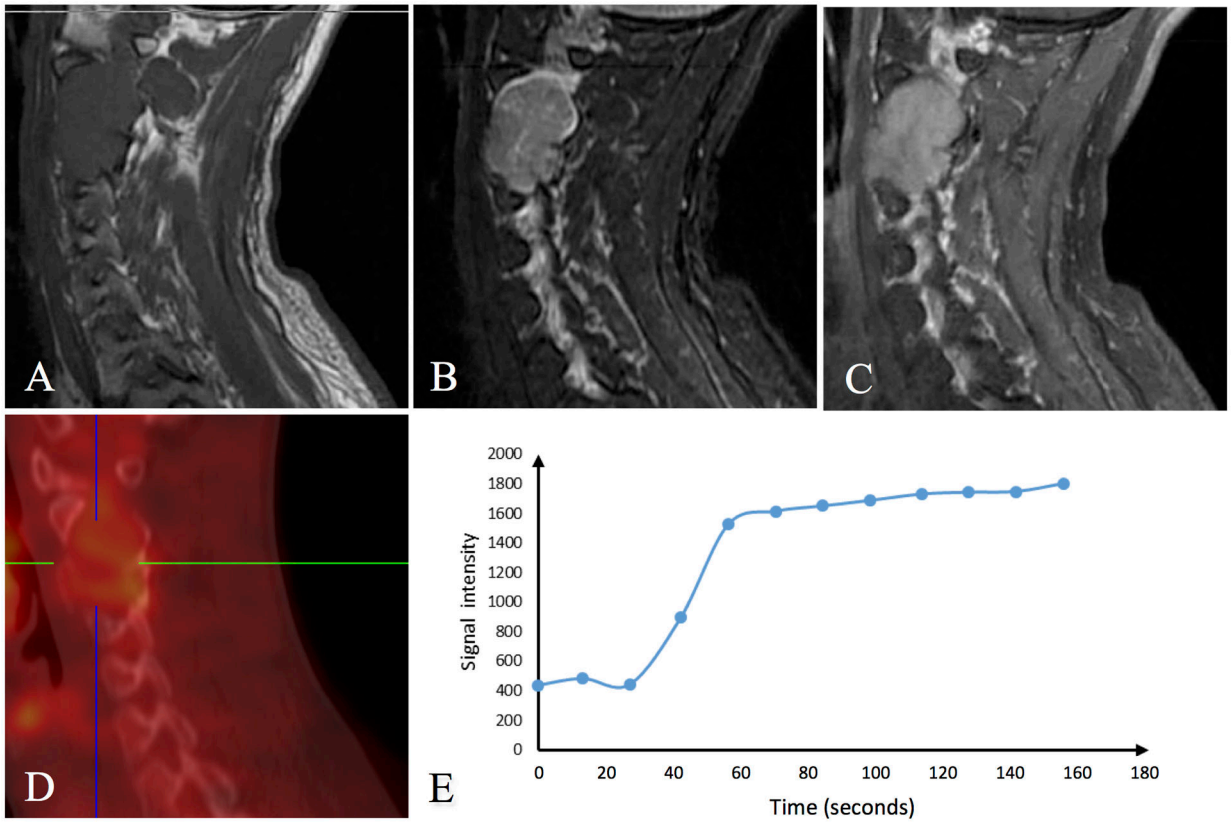

Figure 3.

A 32-year-old male patient with Schwannoma on C1–3. (A) T1-weighted image; (B) T2-weighted fat-suppressed image; (C) T1-weighted contrast-enhanced image; (D) FDG uptake map; (E) DCE signal intensity time course. The anatomic appearance of the lesion is similar on MRI and PET, thus can be identified despite of the low FDG uptake. DCE-MRI enhancement kinetics shows the persistent enhancement pattern, with K^{trans}=0.23 (1/min) and k_{ep}=0.27 (1/min), and the measured SUV_{max}=3.1.

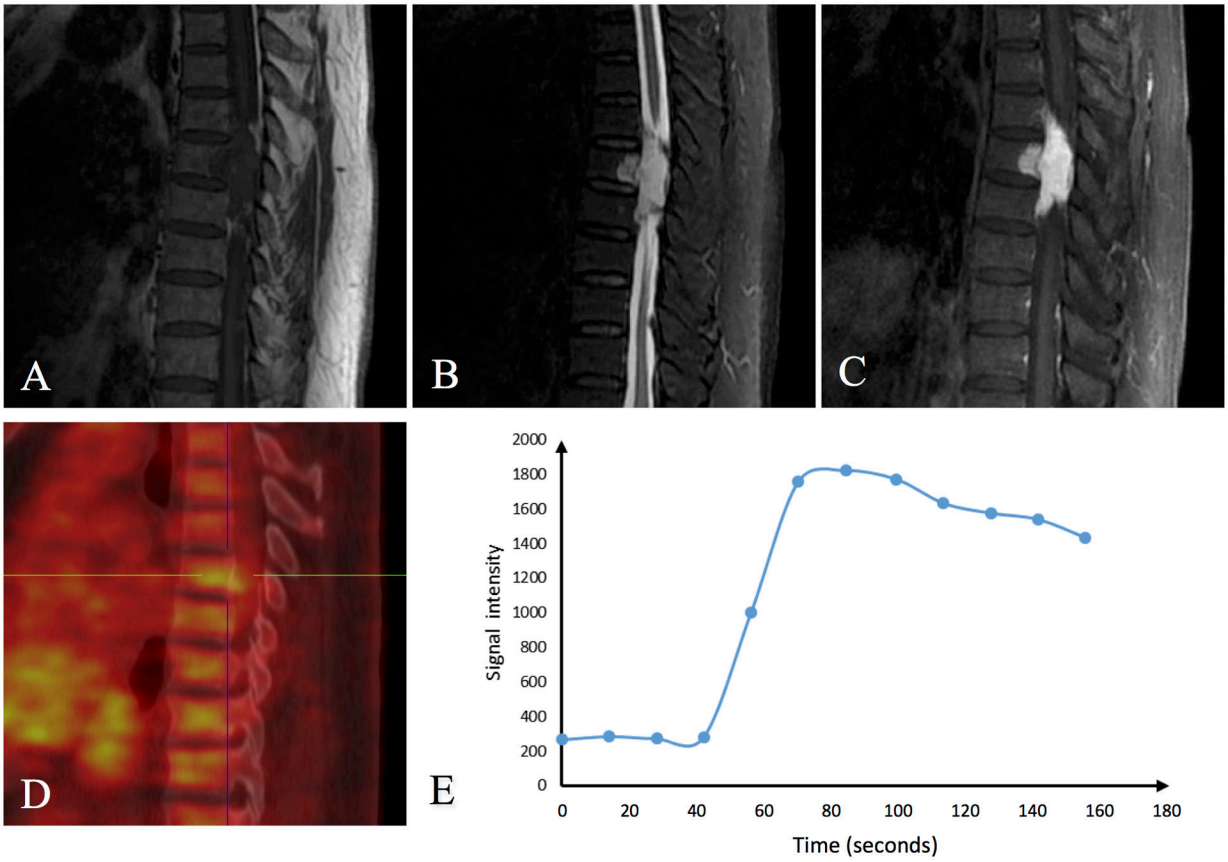

Figure 4.

A 68-year-old male patient with Hemangioma on T7–9. (A) T1-weighted image; (B) T2-weighted fat-suppressed image; (C) T1-weighted contrast-enhanced image; (D) FDG uptake map; (E) DCE signal intensity time course. A low FDG uptake is seen on T7–9, with SUV_{max}=3.7. DCE-MRI enhancement kinetics shows the wash-out pattern, indicating a high perfusion, with K^{trans}=0.62 (1/min) and k_{ep}=0.79 (1/min).

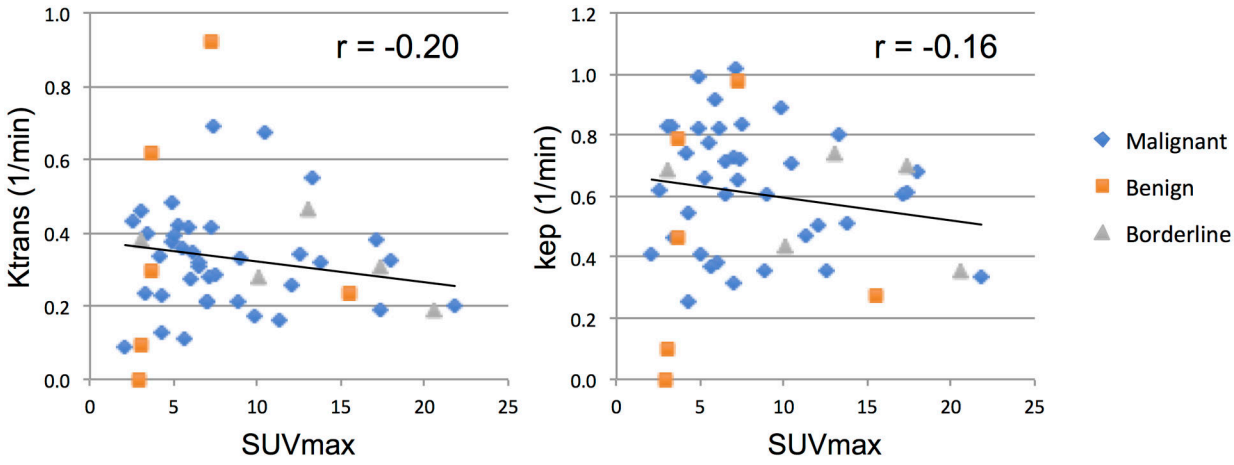

Figure 5.

The correlation plot of K^{trans} (1/min) and k_{ep} (1/min) with SUV_{max}. The correlation is non-significant, showing a weak negative trend with r = −0.20 and −0.16, respectively.

Table 1.

The DCE-MRI and FDG PET/CT parameters in different histological types, and the comparison p values

	K^{trans} (1/min)	k_{ep} (1/min)	SUV_{max}
Malignant (N=38)	**0.32 ± 0.14**	**0.63 ± 0.20**	**8.10 ± 4.72**
Metastasis (N=19)	0.33 ± 0.14	0.61 ± 0.18	9.37 ± 4.26
Plasmacytoma (N=8)	0.32 ± 0.10	0.78 ± 0.17	5.58 ± 2.16
Osteosarcom (N=4)	0.43 ± 0.19	0.56 ± 0.21	9.00 ± 5.58
Lymphoma (N=3)	0.20 ± 0.08	0.57 ± 0.38	11.5 ± 8.92
Chordoma (N=2)	0.24 ± 0.22	0.44 ± 0.04	2.75 ± 0.92
Malignant peripheral schwannoma	0.32	0.60	6.50
Ewing's sarcoma	0.43	0.62	2.50
Benign (N=6)	**0.38 ± 0.32**	**0.50 ± 0.33**	**6.03 ± 4.91**
Hemangioma (N=3)	0.61 ± 0.31	0.74 ± 0.26	3.43 ± 0.46
Schwannoma (N=2)	0.17 ± 0.10	0.19 ± 0.12	5.20 ± 2.97
Giant cell tumor of tendon sheath	0.15	0.39	15.5
Borderline (N=5)	**0.32 ± 0.10**	**0.58 ± 0.17**	**12.82 ± 6.75**
Langerhans cell histosis	0.19	0.35	20.6
Mesenchymal tumor	0.46	0.74	13.0
Osteoblastoma	0.30	0.70	17.3
Giant cell tumor of bone	0.28	0.44	10.1
Solitary fibrous tumor	0.38	0.68	3.10
Group Comparison			
Malignant vs. Borderline vs. Benign P	0.95	0.50	0.11
Metastases vs. Plasmacytoma P	0.87	**0.02** *	**0.03** *
Metastases vs. Plasmacytoma Z	0.17	−2.35	2.38

* significantly different with $p < 0.05$

Table 2.

AUC of k_{ep} and SUV_{max} for differentiation of metastasis and plasmacytoma

Parameter	AUC	Optimal thresholds	The largest Jordan exponent	Sensitivity	Specificity
k_{ep}(1/min)	0.79	0.72	0.61	87.5	73.7
SUV_{max}	0.78	5.70	0.41	78.9	62.5